Geomechanics and Engineering, *Vol. 23, No. 2 (2020) 127-137*
DOI: https://doi.org/10.12989/gae.2020.23.2.127

Experimental research on the evolution characteristics of displacement and stress in the formation of reverse faults

Shao J. Chen[1a], Zhi G. Xia*[2], Da W. Yin[2] and Zhao W. Du[2]

[1]*State Key Laboratory of Mining Disaster Prevention and Control Co-founded by Shandong Province and the Ministry of Science and Technology, Shandong University of Science and Technology, Qingdao, China*
[2]*School of Mining and Safety Engineering, Shandong University of Science and Technology, Qingdao 266590, China*

(Received June 5, 2019, Revised September 11, 2020, Accepted September 26, 2020)

Abstract. To study the reverse fault formation process and the stress evolution feature, a simulation test system of reverse fault formation is developed based on the analysis of reverse fault formation mechanism. The system mainly consists of simulation laboratory module, operation console and horizontal loading control system, and data monitoring system. It can represent the fault formation process, induce fault crack initiation and simulate faults of different throws. Simulation tests on reverse fault formation process are conducted by using the simulation test system: horizontal loading is added to one side of the model. the bottom rock layer cracks under the effect of the induction device. The crack dip angle is about 29°. A reverse fault is formed with the expansion of the crack dip angle towards the upper right along the fracture surface and the slippage of the hanging wall over the foot wall. Its formation process unfolds five stages: compressive deformation of rock, local crack initiation, reverse fault penetration, slippage of the hanging wall over the foot wall and compaction of fault plane. There is residual structural stress inside rock after fault formation. The study methods and results have guiding and referential significance for further study on reverse fault formation mechanism and rock stress evolution.

Keywords: reverse fault formation process; simulation test; system development; fault crack initiation; evolution of stress deformation

1. Introduction

There emerge many geological structures after a long period of tectonic movement of the earth crust. Faults exist as one of the geological structures in strata. The formation of faults destroys the continuity and integrity of rock mass (Anderson 1951). They make the displacement and mechanical feature of the surrounding rock mass be significantly different with the normal one (Xia *et al.* 2020). Thus the surrounding rock mass is characterized as low strength, large deformation and a great amount of hidden deformation energy (Wang *et al.* 2017, Fan *et al.* 2019, Wang *et al.* 2020, Du *et al.* 2020). These features become potential risk factors which may cause mining engineering disasters and threaten mine safety production. For example, faults may induce rock burst, roof collapse, water burst, etc., in mine disasters (Genis *et al.* 2018, Jiang *et al.* 2018, Chen *et al.* 2018, Sainoki and Hani 2014a, Zhang *et al.* 2017, Islam and Shinjo 2009, Donnelly 2006, Lizurek *et al.* 2015, Caine *et al.* 1996, Yukutakea *et al.* 2015). Therefore, the study on fault formation process and its mechanism has great significance for ensuring safety production in mines.

The faults formation needs a long-period of tectonic movement and has the feature of imperceptibility. So it is difficult to conduct long-term monitoring on the stress and displacement and to study fault formation mechanism and its stress deformation evolution based on site investigations. With the in-depth study on geological tectonics, people's understanding of it develops from the qualitative understanding to semi-quantitative and quantitative analysis and study. Tectonophysics model tests can help represent the evolutionary process of geological structure. It is an effective means to further study the formulation feature and mechanism of geological structure. Its test equipment plays an important role in tests (Mcclay *et al.* 2004, Ahmadi *et al.* 2018, Tali *et al.* 2019). According to different geologic origins and typical structural styles, domestic and international scholars have developed tectonophysics model test systems and conducted studies on compressive structure, extensional structure and inverted structure, etc. James Hall firstly puts forward the theory of tectonophysics simulation test and conducts related tests on folds (Zhong 1998). Ghosh *et al.* (1993) carry out simulation studies on superposed folds and deems the mode of superposed buckling in multilayers is essentially controlled by the early shape of folds. Currie (1956) studies the formation process of grabens under the heave background. Mcclay *et al.* (1991) conduct simulation test studies on extensional structure and introduces three extensional tectonic test models. Ji *et al.* (2013) develop a test device for physical models of reverse faults evolution process through selection of model test similarity criteria and the establishment of similitude ratio. Shan *et al.* (1999) study the formation and

*Corresponding author, Ph.D.
E-mail: xzgyy88@163.com
[a]Ph.D.
E-mail: kd_duanceng@163.com

ISSN: 2005-307X (Print), 2092-6219 (Online)

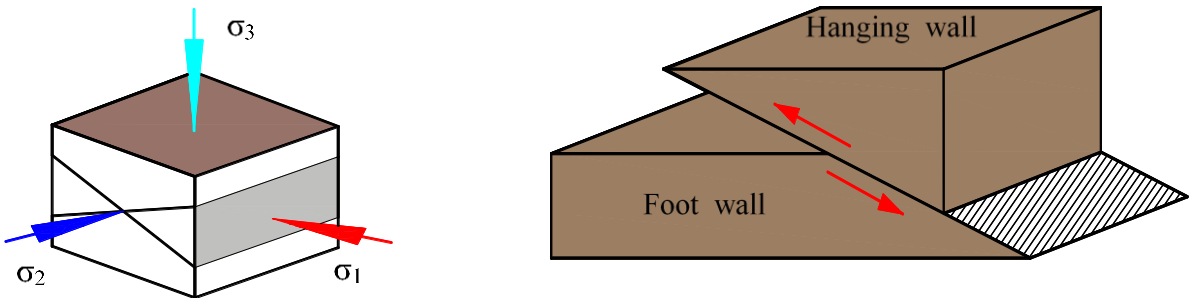

Fig. 1 Stress state diagram of reverse fault formation

evolutionary dynamics of continent-continent collision orogenic belts by applying their self-developed GJ-1 physical simulation test device. Zhou (1999) discusses the influence of boundary geometric property on the formation characters of inverted structure according to his ideal sandbox model of half-graben inverted structure with the geometry properties of rigid boundary and free boundary. Chang *et al.* (2013) proposed a method to calibrate the micro-parameters of materials used in numerical simulations, simulated the reverse faults through a physical model and numerical simulations, and studied the propagation of rock fractures through sand cover and the evolution law of surface deformation. Gazetas *et al.* (2015) carried out experimental and theoretical research on the influences of two types of faults on a large caisson foundation and considered that the failure mechanism of bridge foundation development mainly depends on the type of fault, the precise location of the foundation relative to the fault and the magnitude of fault migration.

Many scholars have done a lot of research on the formation and propagation of reverse faults by using finite element program or discrete element method (Hardy and Finch 2007, Gray *et al.* 2014, Hazeghian and Soroush 2015, Feng and Gu 2017, Nollet *et al.* 2012). Hardy and Finch (2006) used the discrete element model to investigate the influence of sedimentary cover strength on the development of basement-involved fault-propagation folds, and believed that uniformly weak cover best promotes the development of classical. Loukidis *et al.* (2009) studied the propagation of an active dip-slip fault rupture through a uniform soil layer covering the rigid bedrock by using numerical simulation. Hazeghian and Soroush (2017) used a GPU-based DEM modeling methodology with rolling resistance is employed to study comprehensively dip-slip faulting through granular soils from both engineering and fundamental viewpoints. Anastasopoulos *et al.* (2008) developed three different finite element (FE) analysis methods to simulate the propagation of dip slip fault rupture propagation through soil and its interaction with the foundation-structure system. Wyrick and Smart constructed and analyzed two-dimensional discrete element models to test the hypothesis of shallow dike emplacement and widening as a primary mechanism for the production of grabens on Mars.

The above studies have great significance for the understanding of fault formation process and its mechanisms. But the above-mentioned test devices are mainly designed based on certain geological structures, instead of studies on the formation of reverse faults. They simulate only the evolution process of reverse faults, rather than the process of crack initiation and the development process. In addition, in the field of mining engineering, when the physical model is applied to simulate the influence of faults on mining, the laws of fault activation, overlying rock movement and stress evolution caused by mining under pre-existing faults are studied by laying out faults in advance. In contrast, the formation process of faults is yet to be adequately investigated. More importantly, the influence of the existence of tectonic stress and fault fracture zones of the host rock are ignored when the displacement and stress field evolution laws of the rock mass are studied. In fact, previous studies that investigate the influence of mining activity on fault reactivation and rock mass instability did not sufficiently consider the pre-existing stress disturbance and damage zone around faults that had occurred during fault formation process (Jiang *et al.* 2020, Wang *et al.* 2016, Wang *et al.* 2018, Zhao *et al.* 2020, Chen *et al.* 2020). In view of this, a reverse fault formation simulation test system is developed to disclose the reverse fault formation mechanism and fault development and evolution according to Anderson genetic model of fault dynamics (Anderson 1951). The system can completely represent the reverse fault formation process and its fault throw is controllable. Thus it can be used to further study the formation and development process of reverse faults and to obtain the parameters and features of rock deformation, fault development, stress and displacement during the formation process of reverse faults.

2. Reverse fault formation mechanisms

Fault refers to a fracture plane formed in the rock of the earth's crust under the tectonic stress. During the formation process, shear slip occurs to the hanging and foot walls alongside the fault plane. Influenced by the principal stress in the tectonic stress field, different types of faults may have different dip angles. Based on this, scholars established different fault dynamics genetic models according to the relationship between faults and principal stress axis in an homogeneous medium (Xie *et al.* 1991). Anderson applies the Moore-Coulomb strength theory and puts forward the basic theory on mechanical analysis of faults under the premise of equal mechanical properties on all directions of rock. He also explains the stress state of faults. This theory is widely applied and it holds that: in the

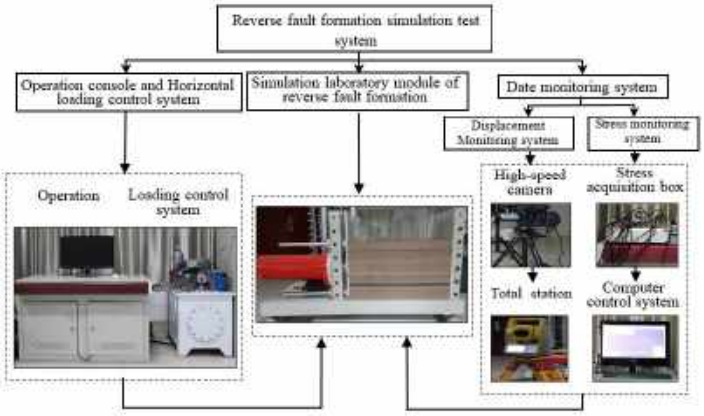

Fig. 2 Reverse fault formation simulation test system

triaxial stress state of a fault, the principal stress tends to be perpendicular to the horizontal plane; the fault plane is a pair of shear fracture planes. σ_1 is consistent with the acute angular bisectrix of the shear fracture planes; σ_3 is consistent with the obtuse angular bisectrix of the shear fracture planes; the walls of the fault slip perpendicularly to the direction of σ_2 (Wang *et al.* 2010, Sun and Zhang 2004).

Reverse fault is formed when the rock ruptures under the effect of horizontal compressional stress. The hanging wall relatively goes up and the foot wall relatively goes down under the compressional stress. Reverse fault is a product of tectonic movement. Most reverse faults are compressive faults. Their fault planes are often slightly wavelike and they have gentle dip angles. Anderson studies the stress state of reverse fault formation according to the Moore-Coulomb Criterion and the basis that the earth surface is a main stress plane (a surface of zero shear stress). That is to say, the reverse fault is formed when the max principal stress axis σ_1 and the secondary principal stress axis σ_2 is horizontal, the min principal stress axis is vertical and the secondary principal stress axis is parallel to the fault strike, see Fig. 1.

The stress standards required for the formation of general reverse faults can be deduced in accordance with Anderson Theory and Moore-Coulomb Criterion. During the formation process of reverse faults, the max principal stress σ_1 is on the hanging wall. It pushes the hanging wall to move upwards. The displacement of the two walls is caused by the movement of the hanging wall. The min principal stress σ_3 in the vertical direction is the gravity of the overlying rock, whose equation is as follows:

$$\sigma_3 = \gamma h \tag{1}$$

After analyzing the stress state of the two axes, the normal stress and the shear stress on the fault plane are described as follows (Wang *et al.* 2010):

$$\sigma_n = \frac{\sigma_1+\sigma_3}{2} + \frac{\sigma_1-\sigma_3}{2}\cos 2\alpha \tag{2}$$

$$\tau = \frac{\sigma_1-\sigma_3}{2}\sin 2\alpha \tag{3}$$

In the above equations, σ_n and τ respectively refer to the normal stress and the shear stress on the fault plane; α refers to the dip angle of the fault plane.

In accordance to the Moore-Coulomb shear fracture criterion, the initial fracture form of the fault plane subjects to the following equation:

$$\tau = S_0 + \sigma_n \tan\phi \tag{4}$$

In the above equation, S_0 refers to the rock cohesion and ϕ refers to the rock internal friction angle.

A equation can be deduced after substituting Eqs. (1), (2) and (3) into Eq. (4):

$$\sigma_1 = \frac{2S_0\cos\phi + \gamma h(1+\sin\phi)}{1-\sin\phi} \tag{5}$$

Two equations can be deduced after substituting Eqs. (1) and (5) into Eqs. (2) and (3):

$$\sigma_n = S_0\cos\phi + \gamma h(1+\sin\phi) \tag{6}$$

$$\tau = \frac{S_0\cos^2\phi + \gamma h\sin\phi\cos\phi}{1-\sin\phi} \tag{7}$$

Eqs. (5)-(7) show the stress required for the formation of general reverse faults. When the rock cohesion s_0 and the internal friction angle ϕ are already known, the required normal stress σ_n, the shear stress τ on the fault plane and the max principal stress σ_1 on the rock can be deduced for the formation of reverse faults.

3. Reverse fault formation simulation test system

In accordance with the dynamic mechanism of reverse fault formation, a reverse fault formation simulation test system is developed. The system mainly consists of simulation laboratory module of reverse fault formation, operation console and horizontal loading control system, and data monitoring system. The reverse fault formation simulation test system, See Fig 2.

3.1 Reverse fault formation simulation laboratory module

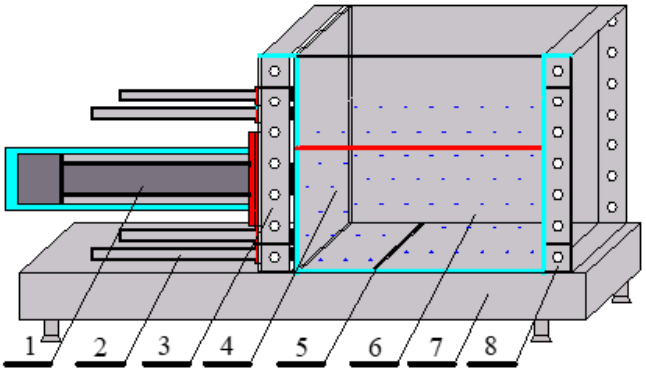

(a) Assembly diagram of the laboratory module

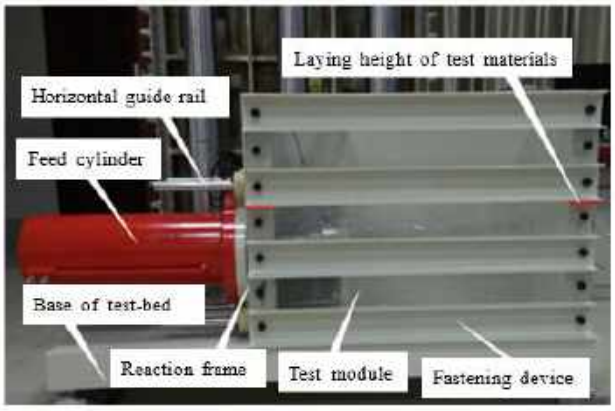

(b) Physical diagram of the laboratory module

Fig. 3 Structural diagrams of the laboratory module

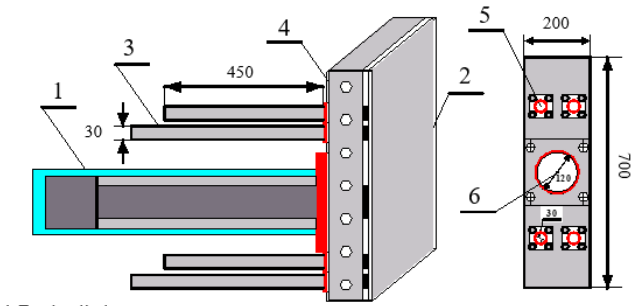

Fig. 4 Structural diagram of loading cylinder and loading pressure head (Unit mm)

Fig. 5 Loading control system

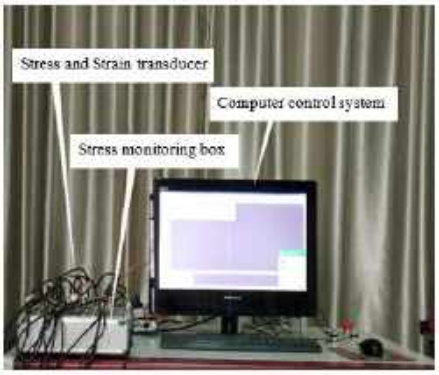

Fig. 6 Stress monitoring system

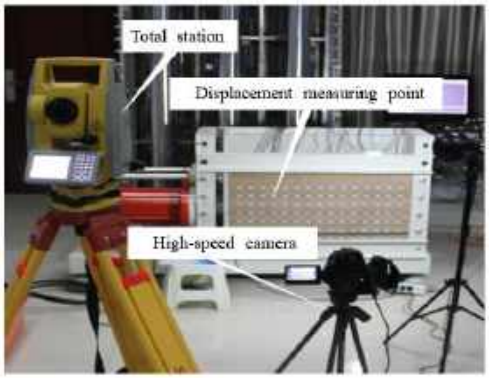

Fig. 7 Displacement monitoring system

The simulation laboratory module of reverse fault formation is composed of two parts: the test module and the base of test-bed. A feed cylinder is installed at the vertical plate at the left side of the laboratory test module. See Fig. 3(a) and 3(b) for the assembly diagram and the physical diagram of the module. The test module is fixed on the base of the test-bed. Its effective simulated size is 800 mm for the length, 300 mm for the width and 700 mm for the height. The real layer height of the simulation materials is 400 mm, as shown the red line in Fig. 3(a). In order to offer a direct observation of rock deformation and fault development during the reverse fault formation process, a 30 mm-thick perspex sheet with high strength and good translucency is adopted as the head board of the test module. In order to further solve the problem of reduced sealing capability due to the deformation of board during the tests, fastening devices are installed at the upper and the bottom of the module to reinforce the head board. The non-deformability of the head board is strengthened. A 20 mm-thick steel plate is adopted as the back board to raise the whole non-deformability of the module. The vertical plates of both sides are fastened to the base of the test-bed to fix feed cylinder, the head and back boards, and the fastening devices.

The base of test-bed is designed to satisfy the structural demands of the test module. The test module is fastened on the top of the base. The base is used to support and fix the

Table 1 Ratio of simulated rocks and similar materials

Rock	Lithology	Sand: Calcium carbonate : gypsum	Gross mass (kg)	Sand (kg)	Lime (kg)	Gypsum (kg)	Water (kg)
R19	Mud rock	9 : 0.6 : 0.4	8.64	7.78	0.52	0.35	0.86
R18	Siltite	8 : 0.6 : 0.4	1.84	1.64	0.12	0.08	0.18
R17	Gritrock	7 : 0.8 : 0.2	7.99	6.99	0.80	0.20	0.80
R16	Mud rock	9 : 0.6 : 0.4	16.63	14.97	1.0	0.67	1.66
R15	Fine sandstone	7 : 0.5 : 0.5	6.3	5.51	0.39	0.39	0.63
R14	Siltite	8 : 0.6 : 0.4	12.49	11.1	0.83	0.56	1.25
R13	Mud rock	9 : 0.6 : 0.4	9.94	8.95	0.60	0.40	0.99
R12	Siltite	8 : 0.6 : 0.4	4.15	3.69	0.28	0.18	0.42
R11	Fine sandstone	7 : 0.5 : 0.5	2.0	1.75	0.13	0.13	0.20
R10	Mud rock	9 : 0.6 : 0.4	15.01	13.51	0.90	0.60	1.5
R9	Fine sandstone	7 : 0.5 : 0.5	7.45	6.52	0.46	0.47	0.75
R8	Siltite	8 : 0.6 : 0.4	3.0	2.67	0.2	0.13	0.30
R7	Coal	9 : 0.6 : 0.4	6.48	5.83	0.39	0.26	0.65
R6	Siltite	8 : 0.6 : 0.4	6.26	5.56	0.42	0.28	0.63
R5	Mud rock	9 : 0.6 : 0.4	4.15	3.74	0.25	0.17	0.42
R4	Fine sandstone	7 : 0.5 : 0.5	1.69	1.48	0.11	0.11	0.17
R3	Siltite	8 : 0.6 : 0.4	8.64	7.68	0.58	0.38	0.86
R2	Gritrock	7 : 0.8 : 0.2	12.79	11.19	1.28	0.32	1.28
R1	Siltite	8 : 0.6 : 0.4	8.28	7.36	0.55	0.37	0.83

test module and serves as the bottom surface of the test module. At the bottom of the base, an anti-slip support is fixed to the ground to make sure that the base won't slip during the tests.

3.2 Lateral loading system

The lateral loading system is composed of feed cylinder, loading pressure, horizontal guide rail, operation console and control system. Fig. 4 shows the structure of the feed cylinder, the loading pressure, the horizontal guide rail and the reaction frame. The feed cylinder is fastened to the reaction frame by connectors and is connected to the loading pressure head. It can conduct continuous loading with constant speed. Its max stroke is 400 mm with the precision of 0.01 mm; its max load can reach 1,000 KN with the precision of 0.01KN. The loading pressure head is designed according to the module structure. It is made of 200 mm×700 mm×20 mm high-strength steel plate. Therefore, a large-area uniform loading of simulation materials can be realized. In order to maintain balance of the loading pressure head during the tests, four round horizontal guide rails, each 450 mm long and 30 mm in diameter, are installed on the left side of the loading pressure head. The horizontal guide rails are fastened through the reaction frame to the loading pressure head by connectors. The reaction frame as the reaction device of the feed cylinder is fastened to the base of the test-bed and is connected to the left vertical plate. Meanwhile, the reaction frame is used to support the horizontal guide rails and the feed cylinder so as to ensure that the load can be exerted to the test objects at constant speed.

The loading control system includes operation console and servo-controlled loading system, as shown in Fig. 5. The servo-controlled loading system is access to computer auto-ontrol during the loading process. Its loading speed is controllable and its loading control precision is high.

The stress monitoring system consists of stress and strain transducer, tress monitoring box and computer control system, see Fig. 6. The stress and strain transducer buried inside the rock is connected to the stress acquisition box. The computer control system is used to conduct real monitoring on the inner stress of the rock.

3.3 Data monitoring system

The data monitoring system mainly includes displacement monitoring system and stress monitoring system. The displacement monitoring system is composed of the total station, the high-speed camera, the displacement measuring points and computer, see Fig. 7. The total station is used to measure and record data of displacement measuring points before and after tests. The high-speed camera is used to shoot the whole test process. The computer is used to conduct software recognition processing.

4. Reverse fault formation simulation test

4.1 Determination of simulation test parameters

According to the similarity theory, the model adopts a geometric similarity ratio of 1:500. The model test size is 800 mm×300 mm×400 mm (Length × Width × Height). The simulation strike is 800 mm long, representing 400 m of

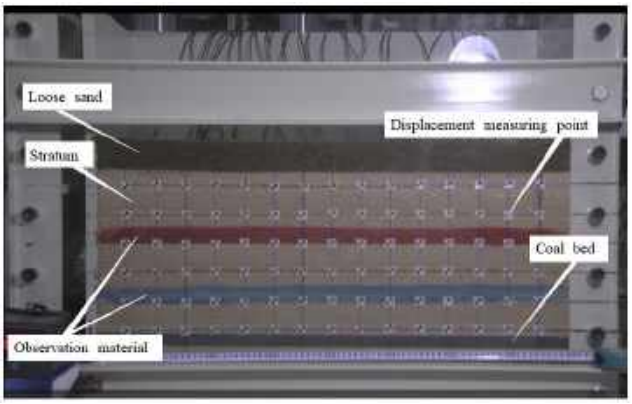

Fig. 8 Layout of the model and displacement

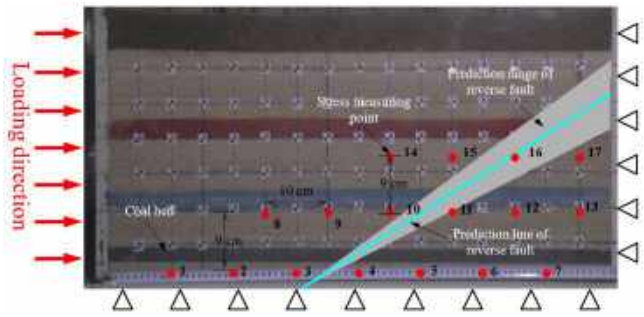

Fig. 9 Layout of pressure sensors measuring points

real strike; the simulation dip is 300 mm long, representing 150 m of real dip; the simulation rock is 400 mm high, representing 200 m of real height. The model simulates that there are 19 layers of rock from the coal floor to the earth's surface. The model is loaded at the speed of 8 mm/min by means of the left horizontal loading device. The front and back, right and bottom boundaries are unmovable. The top of the model is covered with loose sand to simulate the loose layer of the earth's surface.

4.2 Ratios of similar materials

Considering the difference of rock strengths in the earth's crust, simulation materials and their ratio in the mining engineering are adopted for the preparation of simulation materials in the tests (Jiang *et al.* 2015). The volume-weight ratio of similitude is 1:1.5. The simulation materials of coal bed mainly adopt fine river sand as the stuffing, and gypsum, calcium carbonate and water as the cementing materials. These materials are used to simulate rock with different lithology by different ratios (Chen *et al.* 2020). Rock is layered by the mica powder. See Table 1 for the ratio of simulated rocks and similar materials.

4.3 Model preparation

Water is well measured and poured into the well-mixed sand, calcium carbonate and gypsum. Then the well-stirred mixture is poured into the model for compaction. Rock is layered by the mica powder. The time of laying materials should not last too long, in order to avoid evaporation of water during the process. Evaporation of water may influence the mechanical property of similar materials. In order to observe the rock deformation and surface displacement during the process of reverse fault formation, displacement measuring points are placed on the displacement monitoring surface. Red and blue paints are painted and a 50 mm×50 mm mesh is designed on the surface. 90 displacement measuring points are installed at the mesh points, so that the rock movement and fracture situation can be accurately observed during the tests, See Fig. 8.

In order to monitor the internal stress of rock during the process of reverse fault formation, stress measuring points are set up inside the rock. Stress transducers are also installed at the measuring points. According to Anderson's theory on fault dynamics, during the formation of general reverse faults, their fault dip angles are small, about 30°; the fault development does not go along a straight line (Anderson 1951). Based on this, it can be confirmed that, a general development trend and range of the reverse fault, the fault prediction line and the prediction range are as shown in Fig. 9. So the measuring points can be arranged according to the development trend and range of the reverse fault. Inside the model, 17 stress measuring points in 3 rows are arranged. The measuring points of each row are located at the same rock layer. The distance between every two neighboring measuring points in the horizontal direction is 10 cm. The three rows of measuring points are located 9.5 cm, 19 cm and 28.5 cm, respectively, away from the bottom of the model. The left first measuring point of each row is located 10 cm, 25 cm and 35 cm, respectively, away from the left side of the model, See Fig. 9. The bottom rock in the model is blocked from the line of sight by the fastening device, so it is not visible in Fig. 9. But the coal bed and above can be observed from the observation area.

4.4 Experimental method

The loading control system is applied. The unilateral loading mode is adopted to load the model from the left side at a constant speed of 8 mm/min. When the extrusion displacement L=120 mm, the reverse fault is penetrated and compacted. At the very moment, the loading is stopped. During the whole process of the reverse fault formation, a macro monitoring on the rock deformation and fault development is conducted from the transparent head board of the model. Real-time records are made by the high-speed camera; consecutive collections of the horizontal stress inside the rock are completed by using stress and strain transducers.

5. Analysis of the results and discussions

5.1 Rock deformation and fault development rules during the reverse fault formation process

In the simulation test of reverse fault formation, from the beginning of the simulation to the end, the reverse fault formation process is divided into five stages, see Fig. 10(a1)-10(f1): compressive deformation of rock (b1), local crack initiation (c1), reverse fault penetration (d1), slippage

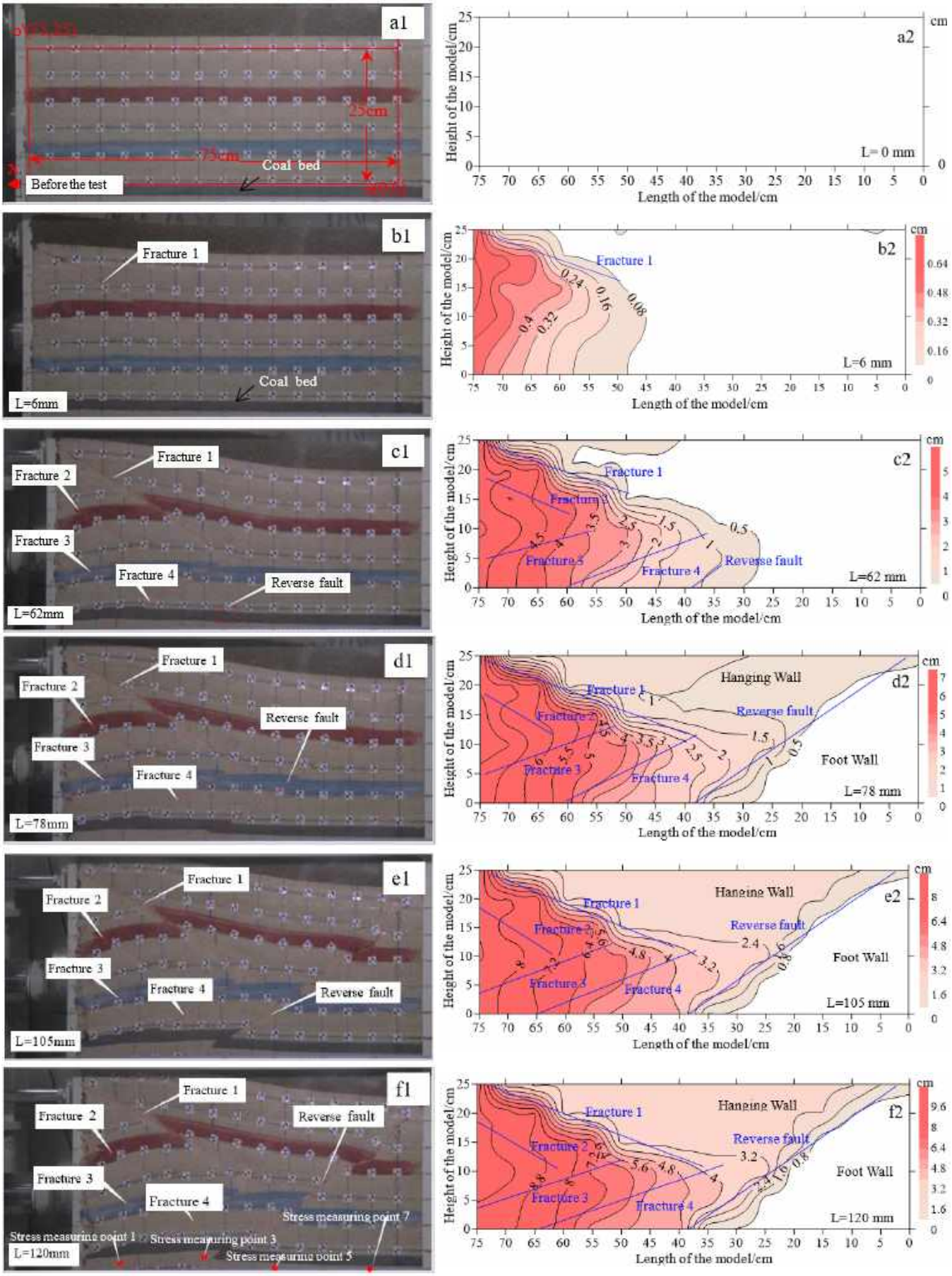

Fig. 10 Deformation features of reverse fault formation

of the hanging wall over the foot wall (e1) and compaction of fault plane (f1). The rock deformation and fault development on the stages of reverse fault formation process and their corresponding horizontal displacement of rock surfaces are as shown in Fig. 10. During the early test, when the extrusion displacement of the left extruded rock L=0 mm~6 mm, it is on the stage of compressive deformation of rock; Fracture 1 firstly develops because the upper left of the model is affected by the surrounding conditions, see Fig. 10(b1). When the extrusion displacement L=6 mm~62 mm, it is on the stage of local crack initiation; the left rock cracks locally, Fractures 2, 3 and 4begin to develop; Fracture 1 of the upper left model continues to develop; its hanging wall slips over the foot wall towards the upper left along the fault plane. As a result, there emerges evident heave on the upper part of rock near the extruded side and folds are formed accordingly; while on the other side, there is less deformation and heave. Meanwhile, the reverse fault develops into the coal bed with a dip angle of about 29°. Fractures 1 and 3 and Fractures 2 and 4 form the shape of ">" respectively, as shown in Fig. 10(c1). When the extrusion displacement L=62 mm~78 mm, it is on the stage of reverse fault penetration. When the extrusion displacement L=78 mm, the reverse fault develops and penetrates into the simulated earth surface under the effect of the inducing device. During this process, fractures of the left rock develops slowly; the fault throw is relatively small, being about 6 mm, as shown in Fig. 10(d1). When the extrusion displacement L=78 mm~105 mm, it is on the stage of slippage of the hanging wall over the foot wall. There is evident slippage between the two walls; the fault throw is relatively large, being about 18 mm. And at the position of about 400 mm from the starting point of fault development, there emerges a large fracture; the fault develops quickly and the dip angle expands largely; this may be because the fracture is formed between the hanging wall and the foot wall under the effect of horizontal stress on the fault and friction force on the fault plane. Influenced by the fracture, the fault development direction is largely changed. Meanwhile, because the hanging wall of the reverse fault slips along the fault plane towards the upper right, there emerges heave on the upper right rock under the effect of nearby forces, as shown in Fig. 10(e1). When the extrusion displacement L=105 mm~120 mm, it is on the stage of compaction of fault plane. The hanging wall of the fault continues to slip upward and the fault throw increases slowly by about 2 mm. And at the position of about 400 mm from the starting point of fault development, the fracture is compacted and the whole reverse fault completes its compression; During the whole process of reverse fault formation, the left fractures develop slowly in the test. Fracture 1 keeps developing but not to the reverse fault, mainly because there is stress release in the whole process. On the stage of compressive deformation of strata, the horizontal extrusion displacement is larger. It accounts for about 1/2 of the whole extrusion displacement in the reverse fault formation process.

The displacement point at the lower right corner of the model is selected as the origin. A range of 75 cm away from the left of the origin along the x-coordinate axis and 25 cm away from the up of the origin along the y-coordinate axis forms a rectangular area, see Fig. 10(a1). Surfer software is applied to conduct inversion on the rock deformation and horizontal displacement in this area during the process of reverse fault formation. Fig. 10(a2)-10(f2) shows horizontal rock displacement cloud pictures during the process of reverse fault formation. Rock is compressed and deformed with the increase of extruded displacement. Fracture 1 develops and moves along the plane; there is evident heave on the upper rock and folds are formed. The horizontal displacement of the model gradually increases; the left rock in the model has the largest horizontal displacement, then the middle and upper rock, and then the foot wall near the fault. The left horizontal extrusion stress and the gravity of the overlying rock is exerted on the foot wall; the fixed boundary on the right restrains the foot wall. Therefore, the low right rock of the foot wall has little change. According to Fig. 10(a2)-10(f2), the horizontal displacement order of different parts of the rock is: the left side of the model, the middle and upper part of the hanging wall, the the foot wall area near the fault, the lower right side of the foot wall.

5.2 The evolution rule of stress at both sides of faults

The fault dip angel formed in the simulation test is about 29°, a little smaller than predicted. But within the prediction range of the reverse fault, the layout of stress measuring points enables observers to monitor the stress on both sides of the fault, as shown in Fig. 9. The stress measuring points 1, 3, 5 and 7 are selected to study the stress evolution rules on both sides of the fault during the process of the reverse fault formation. The measuring points 1 and 3 are located at the hanging wall and the measuring points 5 and 7 are located at the foot wall, as shown in Fig. 10(f1). With regard to measuring points 1, 3, 5 and 7, the relationship between the extrusion displacement and stress increment is shown in Fig. 11: On the stage of compressive deformation of rock, the left rock deforms under the effect of the horizontal extrusion force; the stress increment of all measuring points increases fast; the stress increment of measuring point 1 is faster than that of the other measuring points. On the stage of local crack initiation, fracture develops on the left roe model; the stress increment increases at a slower pace and tends to be stable; when extrusion displacement L=60 mm, the stress increment of measuring point 1 decreases firstly, then the stress increment of the other measuring points decreases in turn from near to far from the extruded side, as shown in the black box in Fig. 11. The main reason is that stress release emerges during the crack development of reverse fault. On the stage of reverse fault penetration, the stress increment of measuring points 1 and 3 on the hanging wall shows a step-like descent; while the stress increment of measuring points 5 and 7 increases for the following factors: firstly, they are located on the foot wall; secondly, the are effected by the horizontal force and the gravity of the overlying rock; thirdly, they are far from the fault. On the stage of slippage of the hanging wall over the foot wall, the stress increment of all measuring points basically keeps stable. The measuring point 3 releases stress earlier and tends to be stable earlier than the measuring point 1 because it is located nearer than the measuring point 1 to the fault. On the stage of compaction of fault plane, the fault plane is compacted by extrusion force and the overlying weight of

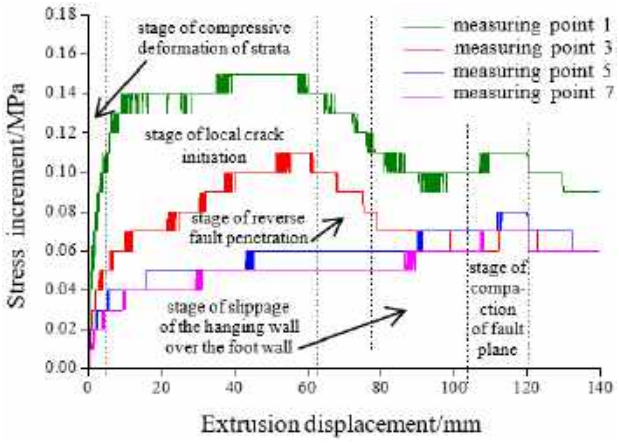

Fig. 11 Variation curve of stress increment on both sides of reverse fault

the foot wall; both the walls sides relative to each other and cause friction; the stress increment of all measuring points increases accordingly. After loading, the stress increment of all measuring points decreases and trends to be stable. The stress increment of the measuring points 3 and 5 near both walls remains 0.06 MPa, which shows that there is residual tectonic stress inside the rock.

The stress increment of measuring points decreases in turn. The stress increment curves of measuring points 1 and 3 have larger fluctuation than those of measuring points 5 and 7. This shows that, for a fault on the same layer, the stress increment of the hanging wall is more obvious than that of the foot wall. From the stage of fault crack initiation to the stage of slippage of the hanging wall over the foot wall, the stress increment gradually decreases and tends to be stable. The stress increment of measuring point 1 reduces by 40% from 0.15 MPa to 0.09 MPa. The stress increment of measuring point 3 reduces by 45.5% from 0.11 MPa to 0.06 MPa. So measuring point 3 has larger decrease amplitude than measuring point 1. Where is nearer to the fault crack initiation position, the release degree of stress is larger and the release speed is faster.

6. Discussion

This paper develops a reverse fault formation simulation test system based on the Anderson's genetic model of fault dynamics. The system is applied to a simulation test on the reverse fault formation to reproduce the formation and development processes of reverse faults. The control of initiation position of reverse faults and fault crack propagation is realized. The rock deformation, fault development and stress evolution rules during the reverse fault formation process are analyzed. The research results have great significance for studies on the dynamics of reverse fault formation, fault crack development, mine disasters prevention during the construction near faults, etc. As geological structure has a strong regional feature, different regions has different tectonic stress fields, strata thickness, lithologic differences, and geographic and geomorphic conditions. This may lead to different rock deformation features, fault dip angles and fault development rules during the reverse fault formation process. The research results in this paper are based on requirements for hard brittle rock with small burial depth and uniform lithology and requirements for the max horizontal stress σ_1 on one side of the model. The top of the model is covered with loose sand to simulate the surface loose layer. The vertical stress on the reverse fault of large burial depth should not be ignored. A certain load should be exerted on the top of the model to simulate the gravity of the overlying rock. In the reverse fault formation simulation test, there emerge two fractures respectively on the upper right part and the low left part near the extruded side. The development of Fracture 1 has a certain influence on the deformation of the left rock of the model. Part of the inner stress of the left rock is released at the same time; this has a certain influence on the deformation of the reverse fault plane. Due to the small size of the model and the influence of model boundary conditions, fractures are formed. In order to study the formation of reverse faults deep in the rock and reduce the influence of model boundary effect, the size of the model should be enlarged; a vertical loading device should be arranged on the top of the reverse fault forming device.

7. Conclusions

• A reverse fault formation simulation test system is developed according to Anderson's genetic model of fault dynamics. The system mainly consists of simulation laboratory module, operation console and horizontal loading control system, and data monitoring system. It has the advantages of simple structure, high-precision loading, real-time monitoring on test data, controllable initiation location of fault crack and fault throw, as well as visualization. The simulation test system is applied to a simulation test on the reverse fault formation to reproduce the formation and development processes of reverse faults. The control of initiation position of reverse faults and fault crack propagation is realized.

• The test preliminarily reveals the rock deformation evolution rules during the reverse fault formation process: with the increase of extrusion displacement, the horizontal displacement increases gradually; compared with the foot wall, there is more evident heave on the upper part of the hanging wall and folds are formed; the left rock in the model has the largest horizontal displacement, then the middle and upper rock, and then the foot wall near the fault; the low right rock of the foot wall has little change. The fault throw is mainly emerged on the stages of reverse fault penetration and slippage of the hanging wall over the foot wall; on the stage of slippage of the hanging wall over the foot wall, the growth rate of the fault throw is larger and more steady.

• From the near to the distant on the loading direction, the stress increment at each measuring point of the same layer decreases in turn; the stress increment at the measuring points of the hanging wall has bigger fluctuation than that of the foot wall. During the early development stage of the reverse fault, when the rock fractures at the

bottom, the stress increment decreases; on the stage of slippage of the hanging wall over the foot wall, where is nearer to the fault, the stress release speed is faster and the stress increment tends to be stable earlier. By the end of loading, the stress increment of all measuring points gradually decreases and tends to be stable; there is residual structural stress inside the rock after the reverse fault is formed.

Acknowledgments

This study was supported by the National Natural Science Foundation of China (51474134, 51774194), Shandong Provincial Natural Science Fundation for Distinguished Young Scholars (JQ201612), Major basic research projects of Shandong Natural Science Foundation (ZR2018ZC07 40), Taishan Scholar Talent Team Support Plan for Advantaged & Unique Discipline Areas.

References

Ahmadi, M., Moosavi, M. and Jafari, M.K. (2018), "Experimental investigation of reverse fault rupture propagation through cohesive granular soils", *Geomech. Energy Environ.*, **14**, 61-65. https://doi.org/10.1016/j.gete.2018.04.004.

Anastasopoulos, I., Callerio, A., Bransby, M.F., Davies, M.C.R., El Nahas, A., Faccioli, E., Gazetas, G., Masella, A., Paolucci, R., Pecker, A.A. and Rossignol, E. (2008), "Numerical analyses of fault–foundation interaction", *Bull. Earthq. Eng.*, **6**(4), 645-675. https://doi.org/10.1007/s10518-008-9078-1.

Anderson, E.M. (1951), *The Dynamics of Faulting*, 2nd Edition, Oliver and Boyd, Edinburgh, U.K.

Chang, Y.Y., Lee, C.J., Huang, W.C., Huang, W.J., Lin, M.L., Hung, W.Y. and Lin, Y.H. (2013), "Use of centrifuge experiments and discrete element analysis to model the reverse fault slip", *Int. J. Civ. Eng.*, **11**(2), 79-89.

Chen, S.J., Du, Z.W., Zhang, Z., Zhang, H.W., Xia, Z.G. and Feng, F. (2020), "Effects of chloride on the early mechanical properties and microstructure of gangue-cemented paste backfill", *Constr. Build. Mater.*, **235**, 117504. https://doi.org/10.1016/j.conbuildmat.2019.117504.

Chen, S.J., Li, Z.Y., Ren, K.Q., Feng, F. and Xia, Z.G. (2020), "Experimental study on development process of reverse fault in coal measures strata and law of stress evolution in hanging wall strata", *J. Min. Safety Eng.*, **37**(2), 366-375. https://doi.org/10.13545/j.cnki.jmse.2020.02.017.

Chen, S.J., Xia, Z.G., Guo, W.J. and Shen, B.T. (2018), "Research status and Prospect of disaster response of rock mass mining under the influence of fault", *Coal Sci. Technol.*, **46**(1), 20-27.

Chen, J.T., Zhao, J.H., Zhang, S.C., Zhang, Y., Yang, F. and Li, M. (2020), "An experimental and analytical research on the evolution of mining cracks in deep floor rock mass", *Pure Appl. Geophys.*, 1-24. https://doi.org/10.1007/s00024-020-02550-9.

Currie, J.B. (1956), "Role of concurrent deposition and deformation of sediments in development of salt-dome graben structures", *Aapg Bull.*, **40**, 1-16. https://doi.org/10.1306/5CEAE2F2-16BB-11D7-8645000102C1865D.

Donnelly, L.J. (2006), "A review of coal mining induced fault reactivation in Great Britain", *Quart. J. Eng. Geol. Hydrogeol.*, **39**(1), 5-50. https://doi.org/10.1144/1470-9236/05-015.

Fan, J.Y., Chen, J., Jiang, D.Y., Wu, J.X., Shu, C. and Liu, W. (2019), "A stress model reflecting the effect of the friction angle on rockbursts in coal mines", *Geomech. Eng.*, **18**(1), 21-27. https://doi.org/10.12989/gae.2019.18.1.021.

Feng, J.W. and Gu, K.K. (2017), "Geomechanical modeling of stress and fracture distribution during contractional fault-related folding", *J. Geosci. Environ. Protect.*, **5**(11), 61-93. https://doi.org/10.4236/gep.2017.511006.

Gazetas, G., Zarzouras, O., Drosos, V. and Anastasopoulos, I. (2015), "Bridge-pier caisson foundations subjected to normal and thrust faulting: Physical experiments versus numerical analysis", *Meccanica*, **50**(2), 341-354. https://doi.org/10.1007/s11012-014-9997-7.

Ghosh, S.K., Mandal, N., Sengupta, S., Deb, S.K. and Khan, D. (1993), "Superposed buckling in multilayers", *J. Struct. Geol.*, **15**(1), 95-111. https://doi.org/10.1016/0191-8141(93)90081-K.

Gray, G.G., Morgan, J.K. and Sanz, P.F. (2014), "Overview of continuum and particle dynamics methods for mechanical modeling of contractional geologic structures", *J. Struct. Geol.*, **59**,19-36. https://doi.org/10.1016/j.jsg.2013.11.009.

Hardy, S. and Finch, E. (2006), "Discrete element modelling of the influence of cover strength on basement-involved fault-propagation folding", *Tectonophysics*, **415**(1-4), 225-238. https://doi.org/10.1016/j.tecto.2006.01.002.

Hardy, S. and Finch, E. (2007), "Mechanical stratigraphy and the transition from trishear to kink-band fault-propagation fold forms above blind basement thrust faults: A discrete-element study", *Mar. Petrol. Geol.*, **24**(2), 75-90. https://doi.org/10.1016/j.marpetgeo.2006.09.001.

Hazeghian, M. and Soroush, A. (2015), "DEM simulation of reverse faulting through sands with the aid of GPU computing", *Comput. Geotech.*, **66**, 253-263. https://doi.org/10.1016/j.compgeo.2015.01.019.

Hazeghian, M. and Soroush, A. (2017), "Numerical modeling of dip-slip faulting through granular soils using DEM", *Soil Dyn. Earthq. Eng.*, **97**, 155-171. http://doi.org/10.1016/j.soildyn.2017.03.021.

Islam, M.R. and Shinjo, R. (2009), "Mining-induced fault reactivation associated with the main conveyor belt roadway and safety of the Barapukuria Coal Mine in Bangladesh: Constraints from BEM simulations", *Int. J. Coal Geol.*, **79**(4), 115-130. https://doi.org/10.1016/j.coal.2009.06.007.

Ji, D.X., Li, P., Su, S.R. and Wang, Y.C. (2013), "Development and application of physical model test device showing evolution process of the reverse fault", *J. Xi'an Univ. Sci. Technol.*, **33**(2), 190-194.

Jiang, J.Q., Wang, P., Jiang, L.S., Zheng, P.Q. and Feng, F. (2018), "Numerical simulation on mining effect influenced by a normal fault and its induced effect on rock burst", *Geomech. Eng.*, **14**(4), 337-344. https://doi.org/10.12989/gae.2018.14.4.337.

Jiang, J.Q., Wang, P., Wu, Q.L. and Zhang, P.P. (2015), "Evolution laws and prediction of separated stratum space under overlying high-position magmatic rocks", *Chin. J. Geotech. Eng.*, **37**(10), 1769-1778. https://doi.org/10.11779/CJGE201510004.

Jiang, L.S., Kong, P., Zhang, P.P., Shu, J.M., Wang, Q.B., Chen, L.J. and Wu, Q.L. (2020), "Dynamic analysis of the rock burst potential of a longwall panel intersecting with a fault", *Rock Mech. Rock Eng.*, **53**, 1737-1754. https://doi.org/10.1007/s00603-019-02004-2.

Jonathan, S.C., Evans, J.P. and Forster, C.B. (1996), "Fault zone architecture and permeability structure", *Geology*, **24**(11), 1025-1028. https://doi.org/10.1130/0091-7613(1996)024<1025:FZAAPS>2.3.CO.

Lizurek, G., Łukasz, R. and Plesiewicz, B. (2015), "Mining induced seismic event on an inactive fault", *Acta Geophysica*, **41**(1), 176-200. https://doi.org/10.2478/s11600-014-0249-y.

Loukidis, D., Bouckovalas, G.D. and Papadimitriou, A.G. (2009), "Analysis of fault rupture propagation through uniform soil

cover", *Soil Dyn. Earthq. Eng.*, **29**(11-12), 1389-1404. https://doi.org/10.1016/j.soildyn.2009.04.003.

Mcclay, K.R. and Scott, A.D. (1991), "Experimental models of hangingwall deformation in ramp-flat listric extensional fault systems", *Tectonophysics*, **188**(1), 85-96. https://doi.org/10.1016/0040-1951(91)90316-K.

Mcclay, K.R., Whitehouse, P.S., Dooley, T. and Richards, M. (2004), "3D evolution of fold and thrust belts formed by oblique convergence", *Mar. Petrol. Geol.*, **21**(7), 857-877. https://doi.org/10.1016/j.marpetgeo.2004.03.009.

Melih, G., Hakan, A., Ömer, A. and Gürkan, B. (2018), "Investigation of possible causes of sinkhole incident at the Zonguldak Coal Basin, Turkey", *Geomech. Eng.*, **16**(2), 177-185. https://doi.org/10.12989/gae.2018.16.2.177.

Nollet, S., Vennekate, G.J.K., Giese, S., Vrolijk, P., Urai, J.L. and Ziegler, M. (2012), "Localization patterns in sandbox-scale numerical experiments above a normal fault in basement", *J. Struct. Geol.*, **39**, 199-209. https://doi.org/10.1016/j.jsg.2012.02.011.

Sainoki, A. and Hani, S.M. (2014), "Dynamic behaviour of mining-induced fault slip", *Int. J. Rock Mech. Min. Sci.*, **66**, 19-29. https://doi.org/10.1016/j.ijrmms.2013.12.003.

Shan, J.Z., Li, J.L. and Xiao, W.J. (1999), "Physical model Experiments of dynamic mechanism on continent-continent collision", *Earth Sci. Front. China Univ. Geosci.*, **6**(4), 399-401.

Sun, Z.Q. and Zhang, J.H. (2004), "Variation of in-situ stresses before and after occurrence of geologic fault structure", *Chin. J. Rock Mech. Eng.*, **23**(23), 3964-3969.

Tali, N., Lashkaripour, G.R., Moghadas, N.H. and Ghalandarzadeh, A. (2019), "Centrifuge modeling of reverse fault rupture propagation through single-layered and stratified soil", *Eng. Geol.*, **249**, 273-289. https://doi.org/10.1016/j.enggeo.2018.12.021.

Wang, C.X., Shen, B.T., Chen, J.T., Tong, W.X., Jiang, Z., Liu, Y. and Li, Y.Y. (2020), "Compression characteristics of filling gangue and simulation of mining with gangue backfilling: An experimental investigation", *Geomech. Eng.*, **20**(6),485-495. https://doi.org/10.12989/gae.2020.20.6.485.

Wang, E.Y., Shao, Q., Du, Y.K. and Han, S.L. (2010), "Genesis mechanism and distribution of Structural coal on two sides of reverse fault", *Min. Safety Environ. Protect.*, **37**(1), 4-6.

Wang, H.W., Jiang, Y.D., Sheng, X., Mao, L.T., Lin, Z.N., Deng, D.X. and Zhang, D.Q. (2016), "Influence of fault slip on mining-induced pressure and optimization of roadway support design in fault-influenced zone", *J. Rock Mech. Geotech. Eng.*, **8**, 660-671. https://doi.org/10.1016/j.jrmge.2016.03.005.

Wang, H.W., Jiang, Y.D., Yang, T., Zhang, D.Q. and Ning, T.H. (2017), "Study on mining induced stress distribution under faults structure", *Coal Eng.*, **48**(1), 92-98.

Wang, P., Jiang, L.S., Li X.Y., Qin, G.P. and Wang, E.Y. (2018), "Physical simulation of mining effect caused by a fault tectonic", *Arab. J. Geosci.*, **11**(23), 741-751. https://doi.org/10.1007/s12517-018-4088-z.

Wu, J.W., Tong, H.S., Tong, S.J. and Tang, D.Q. (2017), "Study on similar material for simulation of mining effect of rock mass at fault zone", *Chin. J. Rock Mech. Eng.*, **26**(S2), 4171-4175.

Wyrick, D.Y. and Smart, K.J. (2009), "Dike-induced deformation and Martian graben systems", *J. Volcanol. Geoth. Res.*, **185**, 1-11. https://doi.org/10.1016/j.jvolgeores.2008.11.022.

Xia, Z.G., Chen, S.J., Liu, X.Z. and Sun, R. (2020), "Strength characteristics and fracture evolution of rock with different shapes inclusions based on particle flow code", *Geomech. Eng.*, **22**(5), 461-473. https://doi.org/10.12989/gae.2020.22.5.461.

Xie, R.H., Qu, T.X. and Qian, G.M. (1991), *Structural Geology*, China University of Mining and Technology Press, Xu Zhou, Jiang Su, China.

Yukutakea, Y., Takeda, T. and Yoshida, A. (2015), "The applicability of frictional reactivation theory to active faults in Japan based on slip tendency analysis", *Earth Planet. Sci. Lett.*, **411**, 188-198. https://doi.org/10.1016/j.epsl.2014.12.005.

Zhang, J., Li, S.C., Li, L.P., Zhang, Q.Q., Xu, Z.H., Wu, J. and He, P. (2017) "Grouting effects evaluation of water-rich faults and its engineering application in Qingdao Jiaozhou Bay Subsea Tunnel, China", *Geomech. Eng.*, **12**(1), 35-52. https://doi.org/10.12989/gae.2017.12.1.035.

Zhao, J.H., Zhang, X.G., Jiang, N., Yin L.M. and Guo, W.J. (2020), "Porosity zoning characteristics of fault floor under fluid-solid coupling", *B. Eng. Geol. Environ.*, **79**(5), 2529-2541. https://doi.org/10.1007/s10064-019-01701-0.

Zhou, J.X. (1999), "Sandbox experimental modeling on the inversion tectonics of Half-Graben", *Prog. Geophys.*, **14**(3), 47-52.

GC